The 8th European Congress on Computational Methods in Applied Sciences and Engineering
ECCOMAS Congress 2022
5-–9 June 2022, Oslo, Norway

EXPLICIT AND IMPLICIT LARGE EDDY SIMULATION FOR A NACA0012 USING A HIGH ORDER DISCONTINUOUS GALERKIN SOLVER

Oscar A. Marino[1], Jon Errasti[1], Esteban Ferrer[1,2], and Eusebio Valero[1,2]

[1] ETSIAE-UPM - School of Aeronautics
Universidad Politécnica de Madrid
Plaza Cardenal Cisneros 3, E-28040 Madrid, Spain

[2] Center for Computational Simulation
Universidad Politécnica de Madrid
Campus de Montegancedo, Boadilla del Monte, 28660 Madrid, Spain

Key words: High Order Methods, NACA0012, turbulence, LES

Abstract. We perform Large Eddy Simulation on a 3D NACA0012 airfoil using a high order discontiuous Galerkin spectral element solver at moderate Reynolds numbers, $Re = 1.0 \cdot 10^5$. The aim is to compare the results of classic explicit Sub Grid Scale models, e.g. the WALE and VREMAN models, with the ones get by using implicit LES, where no explicit SGS is used, but we use stabilising split-form energy-stable formulations, with two-point Pirozzoli and Kennedy-Gruber fluxes. We compare general qualitative variables such as the Q-criteria as well as local quantitative variables, as boundary layer velocity profiles. We show that both methods achive similar predictions for the integrated global variables, but differences can be appreciated in the local velocity profiles.

1 INTRODUCTION

High order methods have been extensively used in computational fluid dynamics due to their accuracy and efficiency in the simulation of fluid flows. This type of discretisation schemes show lower diffusion and dissipative errors and higher numerical accuracy for the same number of degrees of freedom when compared to standard low-order schemes [1, 2, 3]. This characteristic makes them better suited for problems where high accuracy is required.

Since high order methods are able to resolve accurately low to medium wavelenghts, implicit Large Eddy Simulations (iLES) techniques are a good choice for challenging problems at moderate Reynolds numbers. Energy stable formulations have been used to enhance stability of the iLES simulations [4], and have been shown to achieve good predictions of global variables such as lift and drag [5]. This work continues with this idea and explores the prediction capabilities of modelling more detailed variables.

This study aims to asses the numerical predictions a 3D NACA0012 airfoil at a Reynolds of $1.0 \cdot 10^5$ and angle of attack of $4.0°$, using high order techniques. In particular, we compare the results of classic Large Eddy Simulation approaches with the of state of the art iLES simulations using under resolved meshes, namely having a cell size that is coarser than the one need to resolve

the small scales (i.e. Kolmogorov scales). For this, we use a high order discontinuous Galerkin spectral element solver called HORSERS3D and developed at the Dept. of Applied Mathematics of ETSIAE-UPM [6, 7].

2 METHODOLOGY

2.1 High order Discontinuous Galerkin Spectral Element Method

The 3D compressible Navier-Stokes equations can be expressed in the conservative form as

$$\mathbf{q}_t + \nabla \cdot (\mathbf{F}_e - \mathbf{F}_v) = \mathbf{0}, \tag{1}$$

where $\mathbf{q}$ is the vector of conservative variables $\mathbf{q} = [\rho, \rho v_1, \rho v_2, \rho v_3, \rho e]^T$, $\mathbf{F}_e$ and $\mathbf{F}_v$ are the inviscid and viscous fluxes respectively.

To derive a standard Discontinuous Galerkin Spectral Element Method (DGSEM), we consider equation (1) on one mesh element *el*, one can multiply it by a locally smooth test function ϕ_j, typically a polynomial of degree P for $0 \leq j \leq P$, integrate on *el* and, apply the Gauss law on the integral of the flux, obtaining the expresion,

$$\int_{el} \mathbf{q}_t \phi_j + \int_{\partial el} (\mathbf{F}_e - \mathbf{F}_v) \cdot \mathbf{n} \phi_j - \int_{el} (\mathbf{F}_e - \mathbf{F}_v) \cdot \nabla \phi_j = \mathbf{0}, \tag{2}$$

where $\mathbf{n}$ is the normal vector at the element boundaries ∂el. The discontinuous fluxes at inter-element faces can be replaced by a numerical fluxes, $\mathbf{F}_e^*$ and $\mathbf{F}_v^*$, to obtain a weak form for the equations for each element [8],

$$\int_{el} \mathbf{q}_t \phi_j + \int_{\partial el} (\mathbf{F}_e^* - \mathbf{F}_v^*) \cdot \mathbf{n} \phi_j - \int_{el} (\mathbf{F}_e - \mathbf{F}_v) \cdot \nabla \phi_j = \mathbf{0}, \tag{3}$$

the non-linear inviscid and viscous numerical fluxes can be chosen appropriately to control dissipation in the numerical scheme [9, 10]. In this work use the Lax-Friederich flux and the Bassi-Rebay 1 (BR1) [11] scheme respectively.

2.2 Sub-Grid Scale models

Large Eddy Simulation (LES) models are able to resolve turbulent fluctuation up to specific length scales. The principal idea behind LES is to reduce the computational cost of a fully resolved flow (DNS) by modelling the smallest length scales, which are the most computationally expensive to resolve, via low-pass filtering of the Navier–Stokes equations [12]. The large eddies are resolved, whereas the smallest ones can be modelled due to their isotropic behaviour. The effects on the resolved flow due to the smallest eddies are included by means of a so-called sub-grid scale (SGS) model.

The filtered Navier–Stokes equations are similar to the original set of equations, having an extra term, τ_{ij}, which is the SGS stress tensor, and reflects the contribution of the unresolved smallest eddies. As mentioned before, the SGS contribution to the Navier–Stokes equations need to be modeled. Most of the models assume a local equilibrium of the sub grid scales, which is a function of the large scales rate-of-strain tensor (S_{ij}) and a sub grid viscosity (ν_{SGS}), added

to the viscous flux. In that regard, the SGS add dissipation to the Navier–Stokes equations, on the smallest eddies, which are related to the high wave-numbers in the energy spectrum.

Many models SGS have been proposed, being the most famous, the Smagorinsky [13] one. In this work, more advance models are used, such as the Wall-Adapting Local Eddy-Viscosity model (WALE) [14] and the VREMAN model [15].

The complete numerical formulation couples the standard DGSEM with the SGS models, using the Lax-Friederich flux and BR1 scheme for the inviscid and viscous flows respectively. In addition, the polynomial discretization is done using Gauss nodes.

2.3 Implicit LES

Another option to solve the Navier–Stokes equations in a under-resolved spatial discretization is called implicit LES (iLES). The main idea is to rely on the numerical method to add dissipation, instead of using and explicit SGS model. In this case it is important that the numerical dissipation acts in a similar way, adding dissipation only at high wave-numbers.

Riemann solvers are the classic option to include numerical dissipation in DG schemes [16, 17], since they naturally arise when discretising the non-linear terms. However, this dissipation is not enough for high Reynolds number applications, where there could be instability issues, related to aliasing errors [9]. To overcome these problems, stable and energy conserving formulations, mimicking the continuous equations can be included. In our work, we selected split-form discretizations, that are energy preserving [4].

The compressible formulation can be modified by rearranging equation (3), starting by splitting the volumetric integral of the inviscid and viscous fluxes, and applying the Gauss law to the former,

$$\int_{el} \mathbf{q}_t \phi_j + \int_{\partial el} (\mathbf{F}_e^* - \mathbf{F}_e) \cdot \mathbf{n} \phi_j + \int_{el} \nabla \cdot \mathbf{F}_e \phi_j - \int_{\partial el} \mathbf{F}_v^* \cdot \mathbf{n} \phi_j + \int_{el} \mathbf{F}_v \cdot \nabla \phi_j = \mathbf{0}. \tag{4}$$

The required split-form necessitate Gauss–Lobatto points to cancel out boundary terms using the summation-by-parts simultaneous-approximation-term property (SBP-SAT), together with a two-point fluxes, to represent the divergence of the inviscid flux in equation(4). More detail can be found at [18, 4, 19].

For the iLES approach, we keep the same numerical fluxes, namely Lax-Friederich and BR1, being the latter equivalent to the interior penalty formulation when using Gauss-Lobatto points and hexahedral elements [20], as is the case for the present work. In addition, the two-point fluxes used for the inviscid discretization are chosen to be kinetic energy preserving, being the Pirozzoli flux [21], and the Kennedy-Gruber one (KG) [22] two options that are compared in this work. An important remark is the change from Gauss nodes to Gauss-Lobatto nodes (compared to the explicit LES formulation), specially since the former provide higher accuracy [8, 4].

3 SIMULATIONS

3.1 Computational setup

A NACA0012 airfoil section (of constant thickness and chord) with a sharp trailing edge is simulated at a low angle of attack, of $AoA = 4.0°$, using the HORSES3D compressible Navier–Stokes solver and a Reynolds Number (Re) of $1.0 \cdot 10^5$, based on the chord of the airfoil

(C) and the free stream velocity (U_∞), and a Mach Number ($Ma = 0.2$). Periodic boundary conditions on the spanwise direction are imposed.

The computational domain has dimensions of about $22C \times 20C \times 0.1C$, with the leading edge located at $[0, 0, 0]$ (see Figure 1). All the boundary conditions are weakly imposed via Riemann solver. An adiabatic no-slip wall on the airfoil surface; constant and uniform velocity profile of $[v_1, v_1, v_3] = [U_\infty cos(AoA), U_\infty sin(AoA), 0]$ at the inlet (left and bottom boundaries of the domain); and a pressure-based boundary condition is imposed at the outlet (right and top of the domain).

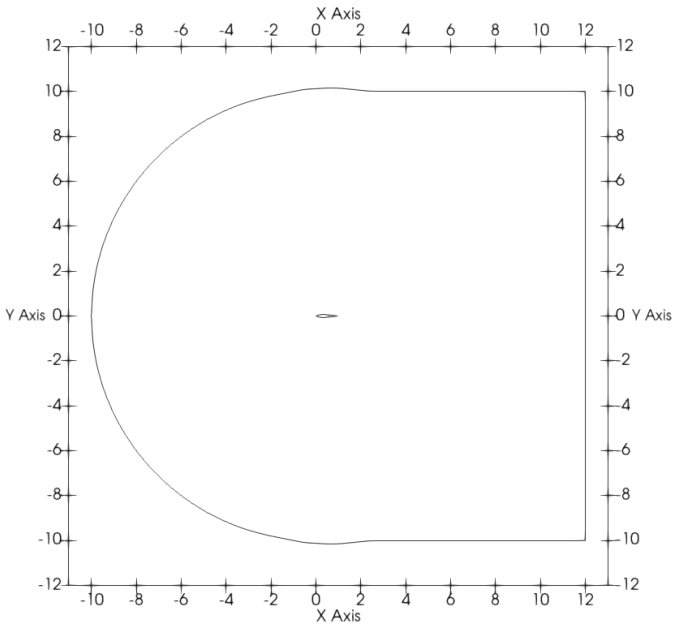

Figure 1: Computational domain and airfoil. Dimensions are defined in terms of chord units (C).

The high order scheme used in this work, employs two different meshes in the discretization of the computational domain. An external structured and hexahedral h-mesh, and an internal p-mesh defining the nodes (based on a Gauss or Gauss-Lobatto nodes) used for the high-order interpolation (see Figure 2 for illustration). The external h-mesh is created using a C-type topology and is conforming. It is constructed extruding uniformly a 2D mesh in the spanwise direction, having this 2D mesh a more refined region near the leading and trailing edge and near the airfoil surface. The 3D h-mesh consists of $23,370$ elements.

The p-mesh uses isotropic polynomial order equals to 3 (4th order accuracy), obtaining a total of almost 1.5 millions degrees of freedom (DoF) in all the cases ($DoF = N_{elem}(p+1)^3$). For the standard DG discretization using SGS, the internal p-mesh is created using Gauss nodes, as seen in Figure 2; while for the split-form discretization used in the iLES case, it uses Gauss-Lobatto nodes (as it is a requirement for the SBP-SAT, see Section 2.3).

The same domain and mesh is used to for the LES with explicit SGS simulation (WALE and VREMAN), and for the iLES simulations, (Pirozzoli and KG two-point fluxes). In all cases

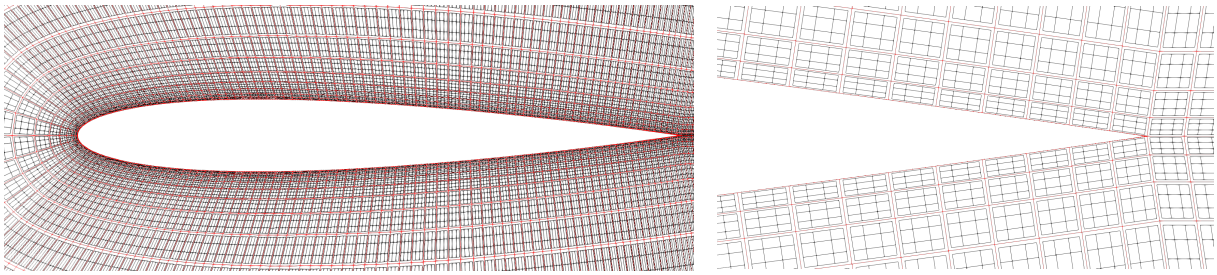

Figure 2: h/p mesh: red lines show coarse h-mesh and black lines the polynomial order 3 (4th order accuracy) mesh using Gauss nodes. left) mesh near the airfoil; right) zoom at the trailing edge zone.

the simulations are advance in time using an explicit 3th order Runge-Kutta scheme, with a Courant-Friederichs-Lewy (CFL) of 0.5. The cases are run until the turbulent flow has fully developed, which typically consists of a convective time units ($T^* = C/U_\infty$) of 70 (starting from a uniform flow field). Afterwards, statistics are gathered for $40T^*$.

3.2 Instantaneous Flow

The instantaneous contour of velocity at the mid-span plane is shown in Figure 3 for the case of iLES using the Pirozzoli flux. The expected behaviour of the flow field can be seen, having a transition from a laminar flow at the vicinity of the leading edge, to a turbulent flow exiting at the trailing edge in the suction side of the airfoil, while the pressure side exhibits a laminar behaviour at the wall of the airfoil.

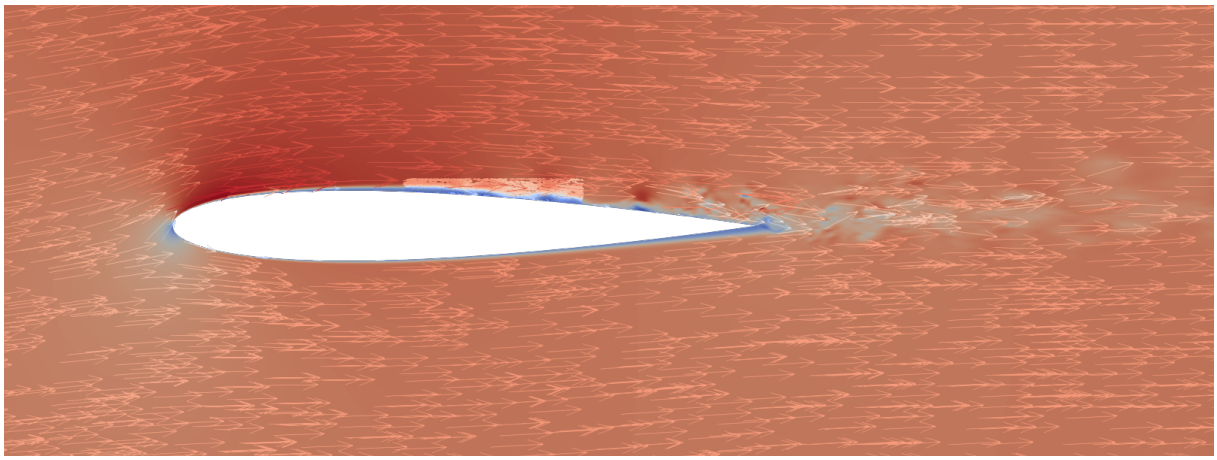

Figure 3: Velocity contour and velocity vectors and the mid-span plane for the iLES Pirozzoli case.

The highlighted zone in Figure 3, the region between x/C 0.4 and 0.6 at the suction side is zoomed in Figure 4, for all the cases. In all but one case (WALE SGS), recirculation flow can be seen, but at very different positions and extensions. For the LES cases with explicit SGS

models, the attachment of the flow is clearer, being the WALE model the first one, showing already no recirculation at this positions. The VREMAN model follows a similar behaviour, being more attenuated, as there is a smaller bubble at $x/C \approx 0.43$. On the other hand, both the iLES models show similar patterns, where several small recirculation bubbles can be observed along the cord.

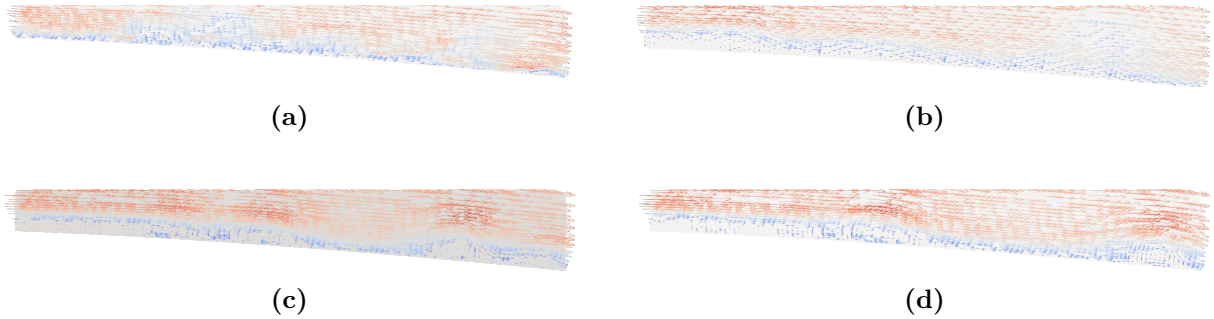

Figure 4: Velocity vectors in region x/C from 0.4 to 0.6: (a) LES with WALE SGS model, (b) LES with VREMAN SGS model, (c) iLES with Pirozzoli flux, and (d) iLES with KG flux.

The differences between each case can also be seen in the 3D flow. Figure 5 shows ,for all the cases, the instantaneous isocountours of the Q-criterion proposed by Hunt et al. [23]. This criterion define turbulent structures where there are positive values of the second invariant of the velocity gradient tensor (Q), which are regions where the rotations are more relevant than the strain. The WALE model predicted the transition to turbulence before mid-cord position, with a very small recirculation zone at in the upstream (at $x/C \approx [0.1, 0.3]$). In contrast, the VREMAN model produces clearer laminar recirculation bubbles that are mostly 2D and evolve into corrugated 3D structures which become later on turbulent structures at the vicinity of the trailing edge. As for the iLES cases, both show the exact behaviour, with a larger 2D laminar separation bubble until transition occurs (at $x/C \approx 0.6$).

Overall we observe that all these LES technique predict a laminar region, transition to turbulence and turbulence separation.

3.3 Time Averaged Flow

To obtain a better understanding of the flow at the boundary layer, the streamwise velocity profiles in the normal direction of the time averaged flows are shown in Figure 6 at different positions along the chord. Averaged and instantaneous flows fields show similar patterns, and show a laminar separation bubble followed by a turbulent profile. The WALE model generates the separation bubble closer to the leading edge and also shows the shortest bubble length. After the mid-chord position, the profile shows a characteristic behaviour of a fully developed turbulent flow. Again, the VREMAN model predicts a more downstream start of the separation, with a slightly longer length. By contrast, the results obtained by the iLES configurations are almost identical, with very small differences, only appreciable at the trailing edge vicinity. The iLES cases predict a similar start of the separation bubble as the VREMAN model, but with a further downstream reattachment.

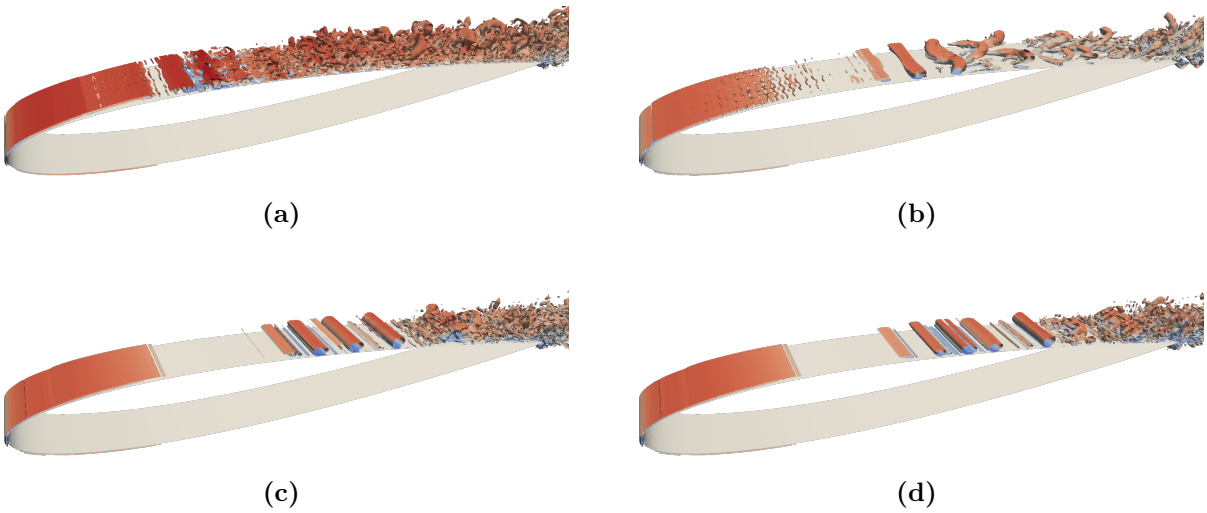

Figure 5: Isocontours of the Q-criterion, coloured by the velocity magnitude. (a) LES with WALE SGS model, (b) LES with VREMAN SGS model, (c) iLES with Pirozzoli flux, and (d) iLES with KG flux.

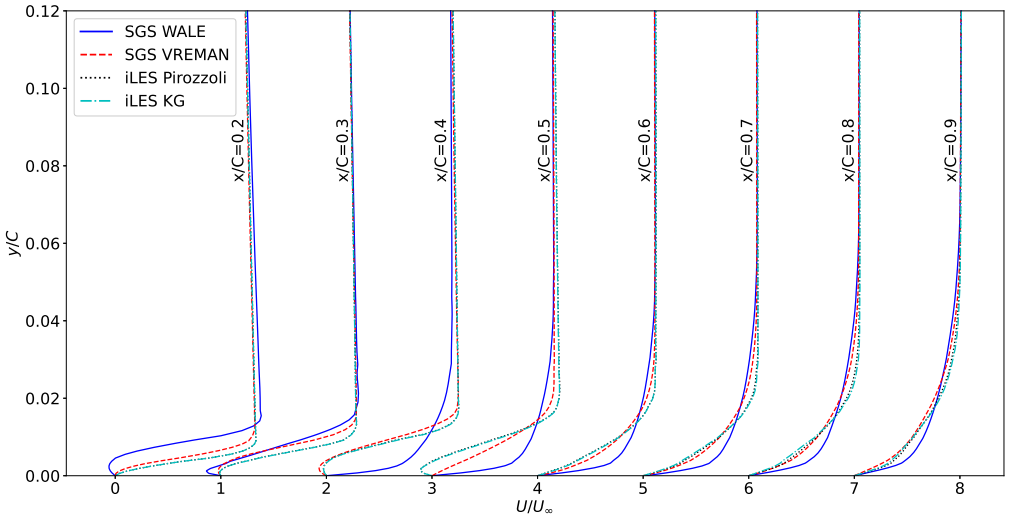

Figure 6: Streamwise velocity profiles of the mean flow in the normal direction.

4 CONCLUSIONS

The 3D turbulent flow simulation of a NACA0012 airfoil at a Reynolds number of $1.0 \cdot 10^5$ and an angle of attack of 4.0° has been performed using a high order discontinuous Galerkin compressible Navier-Stokes solver.

Two different strategies to deal with turbulence in Large Eddy Simulation are used and compared: explicit Subgrid Scale models and energy stable formulations. Both are able to capture the main physics, including the laminar separation bubble and the transition to turbulence.

Differences have been found in the locations of the position of the separation and reattachment, with explicit SGS models providing the smallest length of the bubble, and at a more upstream position. While there are appreciable differences between both SGS models, the WALE and the VREMAN, for the implicit LES, the results of both two-point fluxes, the Pirozzoli and the Kennedy-Gruber are almost identical.

ACKNOWLEDGMENTS

This project has received funding from the European Union Horizon 2020 Research and Innovation Program under the Marie Sklodowska-Curie grant agreement No 860101 for the zEPHYR project. The authors acknowledge the computer resources and technical assistance provided by the *Centro de Supercomputación y Visualización de Madrid* (CeSViMa).

REFERENCES

[1] D. A. Kopriva, "A staggered-grid multidomain spectral method for the compressible navier-stokes equations," vol. 244, pp. 142–158, 1998.

[2] G. E. Karniadakis and S. J. Sherwin, *Spectral/hp element methods for CFD*. OUP, 2005.

[3] C. Canuto *et al.*, *Spectral Methods. Evolution to Complex Geometries and Applications to Fluid Dynamics*. Springer, 2007.

[4] G. J. Gassner, A. R. Winters, and D. A. Kopriva, "Split form nodal discontinuous galerkin schemes with summation-by-parts property for the compressible euler equations," *Journal of Computational Physics*, vol. 327, pp. 39–66, Dec. 2016. DOI: 10.1016/j.jcp.2016.09.013.

[5] E. Ferrer *et al.*, "Implicit large eddy simulations for NACA0012 airfoils using compressible and incompressible discontinuous galerkin solvers," in *Lecture Notes in Computational Science and Engineering*, Springer International Publishing, 2020, pp. 477–487. DOI: 10.1007/978-3-030-39647-3_38.

[6] E. Ferrer *et al.*, *Horses3d: A high-order discontinuous galerkin solver for flow simulations and multi-physics applications*, 2022. DOI: 10.48550/ARXIV.2206.09733. [Online]. Available: https://arxiv.org/abs/2206.09733.

[7] *Numath: Numerical methods in aerospace technology*, [Online; accessed 1-June-2021], 2021. [Online]. Available: https://numath.dmae.upm.es/.

[8] D. A. Kopriva, *Implementing Spectral Methods for Partial Differential Equations*. Springer Netherlands, 2009. DOI: 10.1007/978-90-481-2261-5. [Online]. Available: https://doi.org/10.1007%2F978-90-481-2261-5.

[9] J. Manzanero *et al.*, "Design of a smagorinsky spectral vanishing viscosity turbulence model for discontinuous galerkin methods," *Computers & Fluids*, vol. 200, p. 104 440, Mar. 2020. DOI: 10.1016/j.compfluid.2020.104440.

[10] E. Ferrer, "An interior penalty stabilised incompressible discontinuous galerkin–fourier solver for implicit large eddy simulations," *Journal of Computational Physics*, vol. 348, pp. 754–775, Nov. 2017. DOI: 10.1016/j.jcp.2017.07.049.

[11] F. Bassi and S. Rebay, "A high-order accurate discontinuous finite element method for the numerical solution of the compressible navier–stokes equations," *Journal of Computational Physics*, vol. 131, no. 2, pp. 267–279, Mar. 1997. DOI: 10.1006/jcph.1996.5572. [Online]. Available: https://doi.org/10.1006%2Fjcph.1996.5572.

[12] H. Versteeg and W. Malalasekera, *An introduction to computational fluid dynamics: The finite volume method*, 2nd ed. Prentice Hall, 2007, ISBN: 9780131274983.

[13] J. Smagorinsky, "General circulation experiments with the primitive equations: I. the basic experiment," *Monthly weather review*, vol. 91, no. 3, pp. 99–164, 1963.

[14] F. Nicoud and F. Ducros, "Subgrid-scale stress modelling based on the square of the velocity gradient tensor," *Flow, Turbulence and Combustion*, vol. 62, pp. 183–200, 1999. DOI: 10.1023/A:1009995426001.

[15] A. W. Vreman, "An eddy-viscosity subgrid-scale model for turbulent shear flow: Algebraic theory and applications," *Physics of Fluids*, vol. 16, no. 10, pp. 3670–3681, Oct. 2004. DOI: 10.1063/1.1785131.

[16] Z. Wang *et al.*, "High-order cfd methods: Current status and perspective," *International Journal for Numerical Methods in Fluids*, vol. 72, no. 8, pp. 811–845, 2013. DOI: 10.1002/fld.3767. eprint: https://onlinelibrary.wiley.com/doi/pdf/10.1002/fld.3767. [Online]. Available: https://onlinelibrary.wiley.com/doi/abs/10.1002/fld.3767.

[17] A. D. Beck *et al.*, "High-order discontinuous galerkin spectral element methods for transitional and turbulent flow simulations," *International Journal for Numerical Methods in Fluids*, vol. 76, no. 8, pp. 522–548, Aug. 2014. DOI: 10.1002/fld.3943.

[18] J. Manzanero *et al.*, "Dispersion-dissipation analysis for advection problems with nonconstant coefficients: Applications to discontinuous galerkin formulations," *SIAM Journal on Scientific Computing*, vol. 40, no. 2, A747–A768, Jan. 2018. DOI: 10.1137/16m1101143.

[19] D. A. Kopriva and G. J. Gassner, "An energy stable discontinuous galerkin spectral element discretization for variable coefficient advection problems," *SIAM Journal on Scientific Computing*, vol. 36, no. 4, A2076–A2099, Jan. 2014. DOI: 10.1137/130928650.

[20] J. Manzanero *et al.*, "The bassi rebay 1 scheme is a special case of the symmetric interior penalty formulation for discontinuous galerkin discretisations with gauss–lobatto points," *Journal of Computational Physics*, vol. 363, pp. 1–10, Jun. 2018. DOI: 10.1016/j.jcp.2018.02.035.

[21] S. Pirozzoli, "Numerical methods for high-speed flows," *Annual Review of Fluid Mechanics*, vol. 43, no. 1, pp. 163–194, Jan. 2011. DOI: 10.1146/annurev-fluid-122109-160718. [Online]. Available: https://doi.org/10.1146%2Fannurev-fluid-122109-160718.

[22] C. A. Kennedy and A. Gruber, "Reduced aliasing formulations of the convective terms within the navier–stokes equations for a compressible fluid," *Journal of Computational Physics*, vol. 227, no. 3, pp. 1676–1700, Jan. 2008. DOI: 10.1016/j.jcp.2007.09.020. [Online]. Available: https://doi.org/10.1016%2Fj.jcp.2007.09.020.

[23] J. Hunt, A. Wray, and P. Moin, "Eddies, streams, and convergence zones in turbulent flows," *Studying Turbulence Using Numerical Simulation Databases*, pp. 193–208, Nov. 1988.